Advances in Materials
2021; 10(4): 75-86
http://www.sciencepublishinggroup.com/j/am
doi: 10.11648/j.am.20211004.14
ISSN: 2327-2503 (Print); ISSN: 2327-252X (Online)

Study on the Preparation of Magnetic Pine Needle Biochar and Its Adsorption Performance for the Dye

Zhiyong Han, Dehua Wang, Jie Wu, Qingyue Xiong, Yanxia Zhang, Kaiqing Zhang

College of Petrochemical Engineering, Lanzhou University of Technology, Lanzhou, China

Email address:
hanzhy_009@sina.com (Zhiyong Han)

To cite this article:
Zhiyong Han, Dehua Wang, Jie Wu, Qingyue Xiong, Yanxia Zhang, Kaiqing Zhang. Study on the Preparation of Magnetic Pine Needle Biochar and Its Adsorption Performance for the Dye. *Advances in Materials*. Vol. 10, No. 4, 2021, pp. 75-86. doi: 10.11648/j.am.20211004.14

Received: November 18, 2021; **Accepted**: December 24, 2021; **Published**: December 29, 2021

Abstract: The agricultural and forestry waste pine needle was selected to prepare the biochar which magnetized by the Fe_3O_4 to treat the typical wastewaters of the dye methylene blue (MB) and carmine (P4R) in view of the problem of quick increasing dye wastewater caused by the rapid development of textile, printing and dyeing industries, and the research result showed the experimental values of the maximum adsorption capacity of modified biochar for MB and P4R were 465.6mg·g^{-1} and 336.6mg·g^{-1} respectively. When the dosage of MBC is 0.010g and 0.015g, both the removal rate and the adsorption capacity can be maintained at a high level. Lower pH is conducive to the adsorption of P4R, and a higher pH is conducive to the adsorption of MB. As the adsorption time and initial dye concentration increase, the adsorption capacity of both dyes increases. As the temperature increases, the amount of MB adsorption increases, while the amount of P4R adsorption decreases and the adsorption of MB by MBC is a high-temperature spontaneous adsorption process, and the adsorption of P4R is a low-temperature spontaneous adsorption. The Langmuir model can better describe the adsorption process of MBC to MB, which is a single-layer adsorption, and the Freundlich adsorption model can better describe the adsorption process of MBC to P4R, which is a multi-layer adsorption. The adsorption of MB and P4R by MBC conforms to the quasi-second-order kinetic model.

Keywords: Biochar, Dye Modification, Magnetism, Adsorption, Dye Wastewater, Pine Needle

1. Introduction

Dyes are a kind of organic compounds that can make other substances obtain bright and firm color. Because the pigments used now are synthetic, they are also called synthetic dyes. Dyes and pigments are generally compounds that have their own color and can make other substances obtain bright and firm color in molecular state or dispersed state. Dyes are mainly used to dye materials, most of which are synthetic ones, with firm color adhesion and bright color. They are most widely used in textile, printing and dyeing industries, and also used in chemistry, food, ceramics, plastics, biological research and other industries.

In recent years, with the increase of global population and the development of industry as well as the continuous improvement of people's living standards, the printing and dyeing industry has developed rapidly, and the types production and dye use have also increased sharply.

At the same time the printing and dyeing industry has developed swiftly and the production and use of dyes have also increased quickly.

Meanwhile, the annual discharge of dyes into the ecosystem exceeds 7×10^5t [1]. the Dye wastewater seven times of it, as the harm of water pollution to ecosystem, flows into the environment has attracted people's attention for its high chroma, visibility, carcinogenicity and accumulation [2]. Dyes are mainly used to dye materials, most of which are synthetic ones, with firm color adhesion and bright color. They are most widely used in textile, printing and dyeing industries, and also used in chemistry, food, ceramics, plastics, biological research and other industries [3].

Biochar is a kind of carbon with high carbon content, which is formed by pyrolysis and carbonization of plant tissue and waste, animal tissue and waste, industrial waste, etc. under the condition of hypoxia or limited oxygen [4]. It has huge specific surface area, developed pore structure, rich surface functional groups, anti-decomposition, stable properties, economy and reliability, and is widely used in various fields and it has been a hot issue in the field of

environmental protection and remediation with its preparation, application, performance improvement and improvement of pollutant removal performance are the main research fields, this paper puts forward the viewpoint of treating dye pollutants in water by biochar, studies and discusses the preparation, modification, pollutant removal performance and separation technology and method of biochar were studied deeply in order to provide new ideas and methods for dye wastewater treatment [5].

In this paper, the treatment effect, mechanism and microstructure change of the dye wastewater by the biochar and the improvement of the biochar's adsorption performance were investigated deeply in order to provide new suggestion and method for the dye wastewater effective treatment.

2. Materials and Methods

2.1. The Pine Needle Biochar Preparation

Take an appropriate amount of pine needle powder crushed and sieved through 100 mesh into a beaker and add KOH solution. Immerse and stir on a magnetic stirrer for 12h to allow KOH to fully and evenly adhere, then put it into a centrifugal tube for centrifugation for 30min, remove the upper liquid and dry it at 80°C. Place the dried solid in a corundum boat, raise the temperature to a certain temperature at a heating rate of 5°C/min in N_2 atmosphere with a flow rate of 25ml·L^{-1} for pyrolysis for 2h, take it out after the temperature drops to room temperature, repeatedly filter and wash it with ultrapure water and 1mol·L^{-1} dilute hydrochloric acid until the pH is neutral, dry it at 80°C for standby, and mark the biochar as SBC to obtain KOH modified biochar.

2.1.1. Selection of Optimum KOH Concentration

The raw materials were immersed in 0 mol·L^{-1}, 2 mol·L^{-1}, 4 mol·L^{-1}, 6 mol·L^{-1}, 8 mol·$L^{-1}$and 10 mol·L^{-1} KOH solution at the ratio of 1g:10ml, and stirred. The adsorption effect was used as the standard to explore the influence, and the best concentration of KOH was selected. The modified materials with different concentrations were labeled as 0SBC, 2SBC, 4SBC, 6SBC, 8SBC and 10SBC respectively.

2.1.2. Selection of Optimum Temperature

According to the best preparation conditions obtained in 2.1.1, explore the influence of firing temperature in the range of 600°C, 700°C, 800°C and 900°C, and explore the influence based on the adsorption efficiency, and screen the best preparation temperature.

2.2. Biochar Negative Magnetism

The loading ratio of biochar to Fe_3O_4 is 1:1, that is, 0.5g biochar is loaded with 0.5g Fe_3O_4. Accurately measure 0.583g of $FeCl_3$ and 0.42955g of $FeCl_2$, make the molar ratio of Fe^{3+} to Fe^{2+} 2:1, add 0.5g of 8SBC into a three-necked flask, add 100ml of ultrapure water, stir for 1h under the condition of water bath heating at 60°C with N_2, and ultrasonically disperse for 30min. Add 10ml $NH_3·H_2O$ quickly and continue to stir for 2h under the condition of water bath heating at 60°C. Pay attention to sealing the bottle mouth to reduce the escape of NH_3. After the reaction, the prepared magnetic biochar is separated by a strong magnet, the supernatant is poured off, the solid is repeatedly filtered and washed with ultrapure water, the residual $NH_3·H_2O$ is washed, and the magnetic biochar is dried at 80°C for later use, which is labeled as MBC.

2.3. Adsorption Test

2.3.1. Influence of Adsorbent Dosage

The volume of solution is 50mL, the concentration is 100mg·L^{-1}, the temperature is 25°C, the adsorption time is 2h, the natural pH (the pH of P4R solution is about 6.6, that of MB solution is about 7.8), and the rotating speed of shaking table is 150rpm. The effects of different biochar dosage on the adsorption of MB and P4R are investigated, and the dosage is 0.005, 0.010, 0.015, 0.020 and 0.025g respectively. In the adsorption process, the bottle mouth is sealed with sealing film to prevent the change of solution concentration caused by water evaporation. After the adsorption, measure the absorbance (MB absorption wavelength is 662nm, P4R absorption wavelength is 509nm), and calculate the solution concentration according to the standard curve.

2.3.2. Influence of pH on the Adsorption

Adjust the pH with 1 mol·L^{-1} HCl and NaOH solution, the pH gradient of MB solution is 4, 6, 8, 10, 12 and the pH gradient of P4R solution is 4, 6, 8, 10, 11. Measure the concentration after adsorption after 2 hours.

2.3.3. Adsorption Isotherm and Thermodynamics

The solution volume is 50ml. Different concentration gradients are set, namely 50mg·L^{-1}, 100mg·L^{-1}, 150mg·L^{-1}, 200mg·L^{-1} and 250mg·L^{-1}. The temperature gradients are 15°C, 25°C and 35°C. The dosage of adsorbent is 0.01g, natural pH and shaking table speed is 150 rpm. Due to the limitation of experimental conditions, the sampling time is set for 24h. After 24h, sample and measure the solution concentration C_e, which is the adsorption equilibrium concentration. Calculate the adsorption capacity of the equilibrium adsorption capacity q_e according to the obtained data for fitting the adsorption isothermal model. The adsorption thermodynamics was analyzed.

2.3.4. Adsorption Kinetics

The volume of the solution is 50ml, and the concentration gradient of high, medium and low is set at 50mg·L^{-1}, 100mg·$L^{-1}$and 150mg·L^{-1} respectively. Under the experimental conditions of 25°C, 0.01g adsorbent dosage, natural pH and 150rpm shaking table speed, continuous sampling is carried out. The time points are 1min, 3min, 5min, 10min, 20min, 30min, 60min, 120min, 180min, 360min, 720min and 1440min. Measure the solution concentration Ct, that is, the concentration at time T. Calculate the adsorption quantity qt at time T according to the obtained data. Used to fit the adsorption kinetic model.

3. Results and Discussion

3.1. The Optimum KOH Concentration for Biochar Preparation

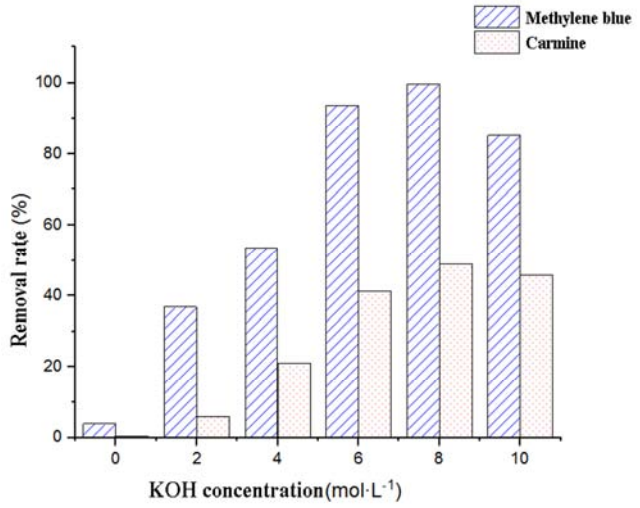

Figure 1. *The influence of different KOH concentrations on the removal rate.*

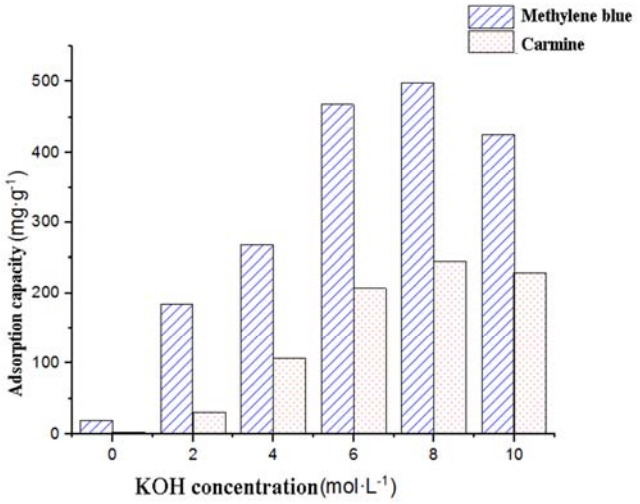

Figure 2. *The influence of different KOH concentrations on the adsorption capacity.*

As can be seen from Figure 1 and Figure 2, with the increase of KOH concentration, the removal rate and adsorption capacity of biochar to the two dyes show a trend of first increasing and then decreasing. The adsorption effect of 8SBC with KOH concentration of 8 mol·L^{-1} is good, and the removal rate and adsorption capacity of MB and P4R reach 99.69% and 498.45 mg·g^{-1}, 49.2% and 246 mg·g^{-1} respectively which certificate that KOH modification can greatly improve its adsorption performance.

In the impregnation process, KOH will erode the pine needle structure to a certain extent, and will react with substances in raw materials such as lignin, etc. With the increase of KOH concentration, more KOH can react with impurities in raw materials, which can be completely removed, and the rest can react with impurities and be removed during carbonization. Etching is carried out on the surface of carbon skeleton. The higher the concentration, the higher the etching degree and the better the hole-making effect [6]. With the increase of KOH concentration, biochar will be excessively etched and its structure will be destroyed, which may lead to the collapse of its pore structure and reduce the specific surface area, but it is not conducive to the improvement of adsorption effect, such as 10 mol·L^{-1} 10SBC. Therefore, the KOH concentration of 8 mol·L^{-1} is appropriate, which will not cause insufficient modification. And will not be excessively damaged [7].

3.2. Optimum Temperature of Biochar Preparation

The effect of preparation temperature on the properties of biochar is shown in Figures 3 and 4.

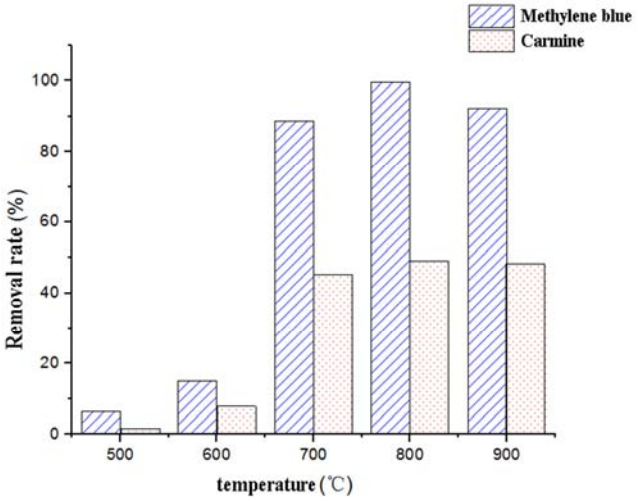

Figure 3. *The influence of different carbonization temperatures on the removal rate.*

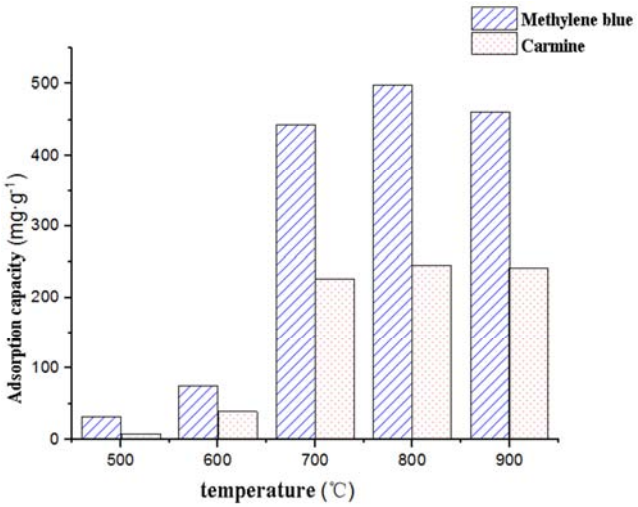

Figure 4. *The influence of different carbonization temperatures on the adsorption capacity.*

As shown in Figures 3 and 4, with the increase of carbonization temperature, the removal rate and adsorption capacity of the modified biochar to the two

dyes show a trend of first increasing and then decreasing, among which biochar fired at 800°C has the optimum adsorption effect. The removal rate and adsorption capacity of MB and P4R were 99.69% and 498.45 $mg \cdot g^{-1}$, and 49.2% and 246 $mg \cdot g^{-1}$ respectively. With the increase of temperature, Impurities of raw materials are removed and carbonized more thoroughly. When the temperature rises from 600°C to 700°C, the effect is improved significantly. At higher temperature, impurities that are difficult to remove at low temperature can be gradually removed under the action of KOH, and the etching effect on carbon skeleton is more significant. When the temperature is too high, the pore structure will collapse, which is not conducive to the formation of pore structure. Reducing its specific surface area leads to the decline of adsorption effect. Therefore, 800°C can completely remove impurities without excessively damaging the structure, which is the optimum firing temperature [8, 9].

3.3. Material Characterization

3.3.1. Analysis of Specific Surface Area

The specific surface area of commercial activated carbon, unmodified activated carbon, modified activated carbon and magnetic biochar were analyzed respectively, and the data are shown in Table 1.

Table 1. *Pore structure data of commercial activated carbon, 0SBC, 4SBC, 8SBC and MBC.*

Material	Specific surface area (m^2/g)	Total pore volume (cm^3/g)	Total pore volume (nm)
Commercial activated carbon	297.5448	0.285002	6.1383
0SBC	0.6654	0.002604	22.8875
8SBC	1145.1521	0.645119	3.8175
MBC	785.7522	0.590631	82.972

It can be seen from the table that after modification, the data of specific surface area and total pore volume are better than those of unmodified biochar, and MBC is lower than 8SBC. After modification, the impurities were removed by KOH, and holes were etched on the carbon skeleton, which increased the specific surface area and total pore volume, which was beneficial to the improvement of its adsorption effect. After negative magnetism, a large number of Fe_3O_4 particles are attached to the surface of biochar. It occupies a certain space, which can be verified by SEM photographs, resulting in the decrease of its specific surface area and total pore volume compared with 8SBC.

3.3.2. Pore Size Distribution

Figures 5-7 shows the pore size distribution and adsorption-desorption curves of 0SBC, 8SBC and MBC:

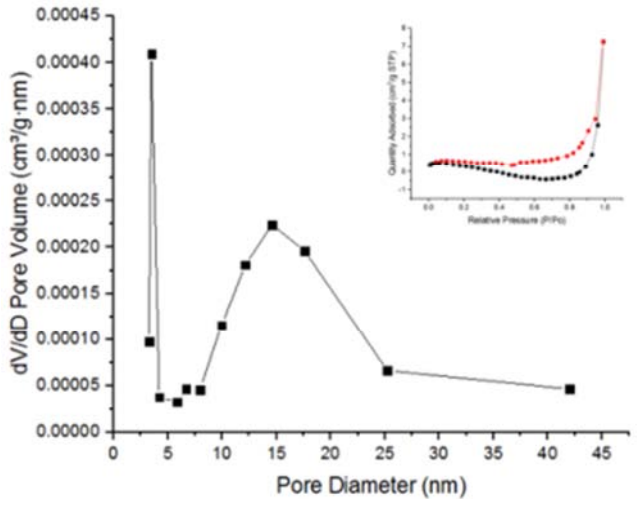

Figure 5. *0SBC pore size distribution diagram and adsorption-desorption curve.*

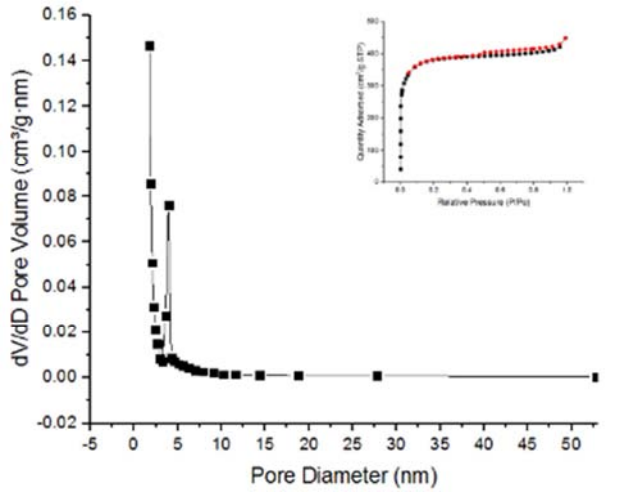

Figure 6. *8SBC pore size distribution diagram and adsorption-desorption curve.*

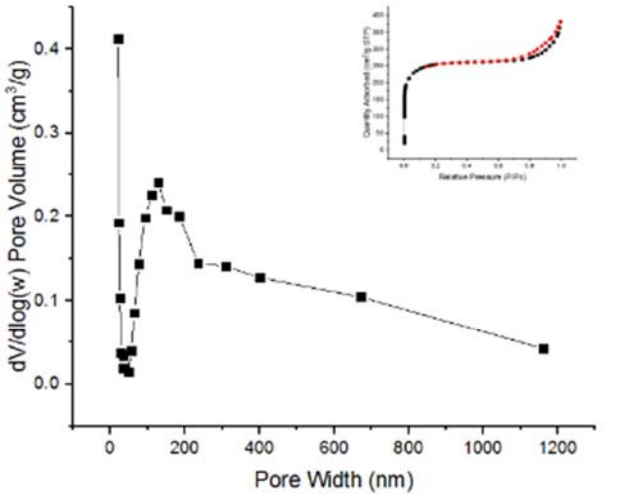

Figure 7. *MBC pore size distribution diagram and adsorption-desorption curve.*

It can be seen from Figure 5 that the adsorption-desorption curve of 0SBC belongs to the mixed isotherm of type II and type IV, and the H4 hysteresis loop. Mainly occurs in mesoporous materials, with an average pore size of 22.89 nm. In the pore size distribution diagram, the pore size is mainly distributed between 10-25 nm, and there are some mesopores close to micropores. However, the content of both of them is very small, and the pore structure is underdeveloped, which is the reason why they are smaller than the surface. It can also be verified by scanning electron microscope observation [10].

As shown in Figure 6 and Figure 7, after modification, the pore structure of 8SBC is more abundant, MBC is prepared on the basis of 8SBC, and the adsorption-desorption curves of both are similar in type, belonging to the mixed isotherm of type II and type IV, and H4 hysteresis loop. Different from HBC, MBC and 8SBC have more developed mesoporous structures. The sharp increase of adsorption capacity in the low-pressure area indicates that there are some micropores. From the pore size distribution diagram, 8SBC is mainly micropores and mesopores with smaller pore sizes, with an average pore size of 3.82 nm. After negative magnetism, the pore structure of micropores was destroyed to some extent, which led to the enlargement of pore size, the increase of mesopore content and the widening of pore size distribution. MBC was mainly mesopore and macropore, with an average pore size of 82.98 nm.

3.3.3. Scanning Electron Microscope Observation

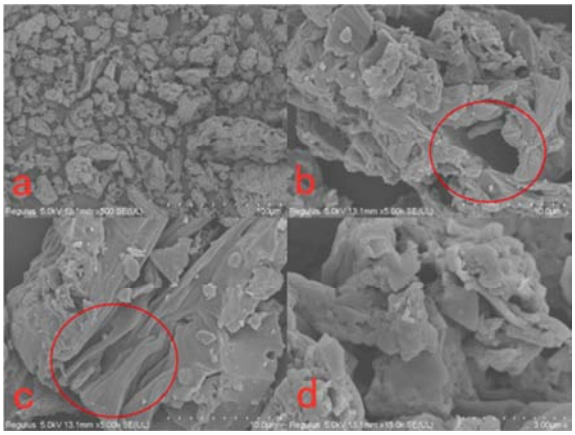

Figure 8. *Scanning electron micrographs of 0SBC: a-500 times magnification, b-5000 times magnification, c-5000 times magnification, d-15000 times magnification.*

As can be seen from Figure 8-a, 0SBC presents irregular granules with different sizes and shapes. Figure 8-b is a photo magnified to 5000 times. The surface of 0SBC is uneven, the structure is messy, and there are no channels, depressions and other structures on the surface. The channel in the red circle is the fiber bundle structure of pine needles, which can provide limited specific surface area. Figure 8-c is a photograph of other parts magnified 5000 times, showing that there are gullies on the surface. Similarly, the contribution of contrast surface area is limited. Figure 8-d is a partially enlarged photograph of Figure 8-b to 15000 times, with rough surface and compact texture. Generally speaking, 0SBC does not have a structure that can provide a large specific surface area, which is also the reason for its small specific surface area [11].

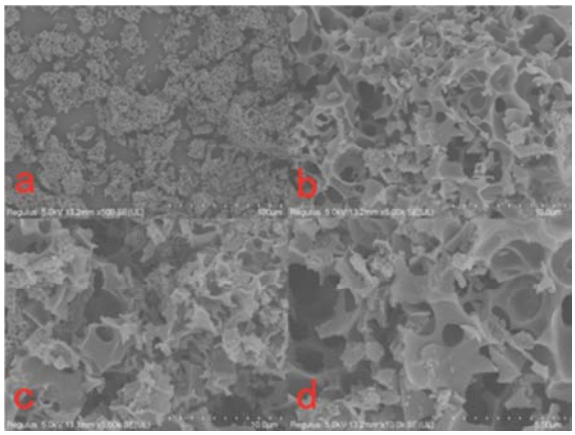

Figure 9. *Scanning electron micrographs of 8SBC: a-500 times magnification, b-5000 times magnification, c-5000 times magnification, d-10000 times magnification.*

It can be seen from Figure 9-a that 8SBC presents irregular granules with different shapes and sizes. The sample is magnified to 5000 times. As shown in Figure 9-b, 8SBC is extremely irregular in shape, full of various channels and depressions, and the structure is fragmented. Figure 9-c is a photograph of other parts magnified to 5000 times, and the fragmentation is more obvious, and the structural wall is relatively thin, which is caused by the etching of KOH. From the outside, KOH etches the outer layer structure sufficiently, the outer layer of the structure is fragmented, and the pore structure mainly exists in the interior. As shown in the red circle of Figure 9-d, similar to QBC, there may be crisscrossing pore structures inside, which form a huge specific surface area and provide a large number of adsorption sites and spaces. If the concentration of KOH continues to increase, the etching effect of KOH on materials will be stronger. The damage of the structure will be more serious, which will not provide enough sites and space for adsorption [12].

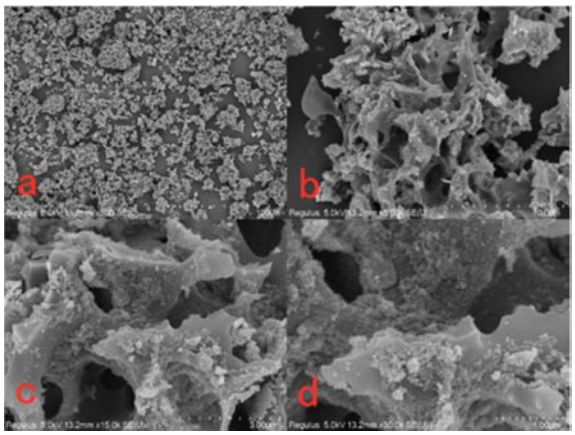

Figure 10. *Scanning electron micrographs of MBC: a-500 times magnification, b-5000 times magnification, c-15000 times magnification, d-30000 times magnification.*

Figures 10-a, b, c and d are the electron microscope photos of MBC with magnification of 500 times, 5000 times, 15000 times and 30000 times respectively. The overall structure of MBC is similar to that of 8SBC. It can be seen that the surface of MBC is covered with a large number of Fe_3O_4 particles, which are successfully loaded on the surface of biochar. The particles gather together due to magnetism, and the overall distribution is not uniform. According to the photo, the particle size of Fe_3O_4 is less than 1μm, which is mainly dispersed and attached to the outer structure of MBC. There are fewer internal channels. The reason is that when Fe_3O_4 particles are formed, the reaction speed is faster, and they are immediately attached to the surface of 8SBC. It takes time to diffuse into the internal channels, and they are also attracted by the magnetic attraction of external particles, so it is difficult to enter the internal channels [13].

3.3.4. X-ray Diffraction Test

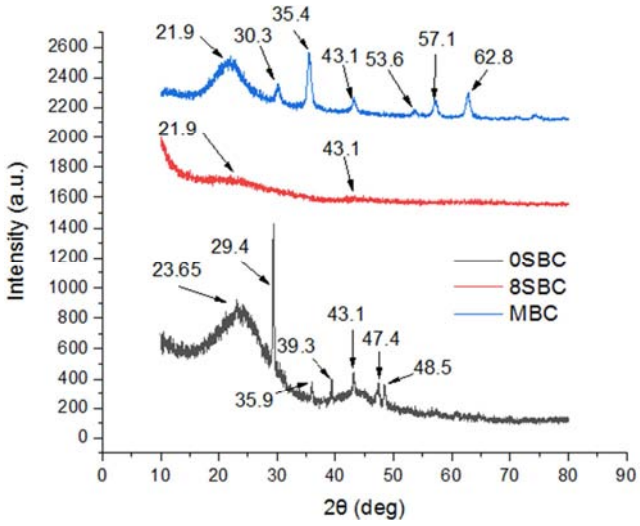

Figure 11. *XRD test spectrum of 0SBC、8SBC and MBC.*

As shown in Figure 11, there are diffraction peaks in 2θ=20 and 2θ=43.1 for 0SBC, 8SBC and MBC, which correspond to the diffraction peaks of (002) and (100) crystal planes of graphite, and the peak type is wide and the intensity is not high, which indicates that the graphitization degree of the material is not high. Compared with ICDD standard card (00-005-0586), the peaks of 0SBC at 2θ=35.9, 39.3, 47.4 and 48.5 are diffraction peaks of $CaCO_3$, which shows that Ca in 0SBC is fired at high temperature to form $CaCO_3$ crystals, but after KOH modification, the diffraction peak of 8SBC about Ca disappears [14]. Compared with 0SBC, 8SBC has a higher degree of disorder, and the presence of amorphous carbon can increase the specific surface area, in accordance with the law of BET test [15]. After the negative magnetization of 8SBC, the crystal structure is more orderly, and the diffraction peaks of Fe_3O_4 appear at 2θ=30.3, 35.4, 53.6, 57.1 and 62.8. Combined with SEM photos and EDS analysis, it is shown that Fe_3O_4 has been successfully loaded on the surface of biochar.

3.3.5. Fourier Transform Infrared Spectrum Analysis

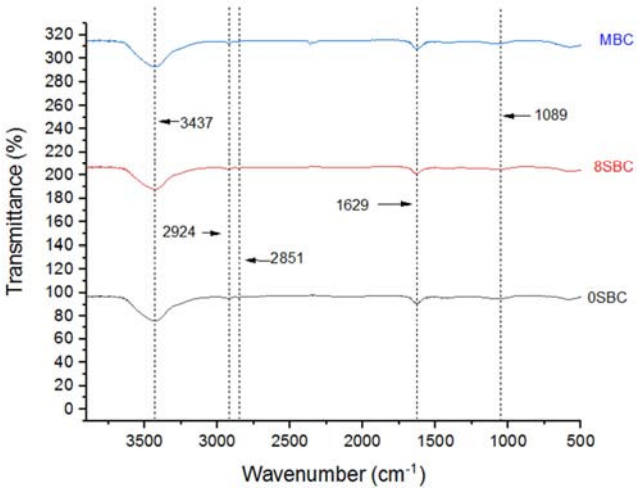

Figure 12. *FTIR spectra of MBC, 8SBC and 0SBC.*

According to Figure 12, there is an obvious absorption peak at 3437cm^{-1}, which is the stretching vibration absorption peak of -OH associated with hydrogen bond. The peaks at 224 cm^{-1} and 2851cm^{-1} are asymmetric stretching vibration and symmetric stretching vibration of C-H. The peak at 629 cm^{-1} is the N-H shear vibration of primary amine, and the peak at 1089 is the stretching vibration of C-O. Generally speaking, the types of functional groups have little change before and after modification [16].

3.4. Study on Adsorption Performance

3.4.1. Influence of Dosage

It can be seen from Figure 13 that with the increase of biochar dosage from 0.005g to 0.025g, the removal rate of MB also increases and gradually flattens out, but the adsorption amount shows a downward trend, with a rapid decline between 0.05-0.015g and a slow decline at the back end.

With the increase of dosage, the materials available for adsorption in the solution increased, which increased the chance of dye molecules contacting biochar, that is, the adsorption sites for binding increased, so the removal rate showed an upward trend, and the removal rate reached 97.53% from 0.01g, and the adsorption amount reached 486.6 mg·g^{-1}. The adsorption equilibrium was reached after 2 hours of continuous increase of dosage, and the curve became flat. The increase of dosage means that less dyes can be adsorbed by biochar per unit mass, which leads to the decrease of adsorption capacity. For MBC adsorption MB system, when the solution volume is 50ml, the concentration is 100mg·L^{-1}, the temperature is 25°C, and the optimal dosage is 0.01g.

For the P4R, it can be seen from the Figure 14 that with the increase of dosage, the removal rate will increase, and the adsorption capacity will first increase and then decrease, reaching the maximum of 311.6 mg·g-1 when the dosage is 0.015g. With the increase of dosage, the number of sites available for adsorption increased, and the removal rate also

increased, and the removal rate reached 93.49% at 0.015g. When the dosage is between 0.05g-0.015g, the dosage is relatively low. A unit mass of adsorbent can adsorb a large number of dyes, so the adsorption capacity also increases. When the total amount of dye molecules in the adsorption system is constant, the dosage continues to increase, and the adsorbable dyes per unit mass of biochar rapidly decrease, leading to the decrease of adsorption capacity. Therefore, in this subject, for the MBC P4R adsorption system, when the solution volume is 50ml and the concentration is 100 mg·L-1, the temperature is 25°C and the dosage is 0.015g are ones ofthe optimal adsorption conditions.

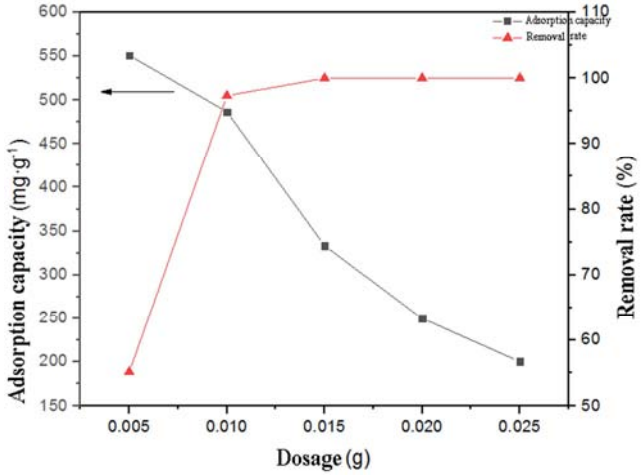

Figure 13. *The effect of MBC dosage on the removal of MB.*

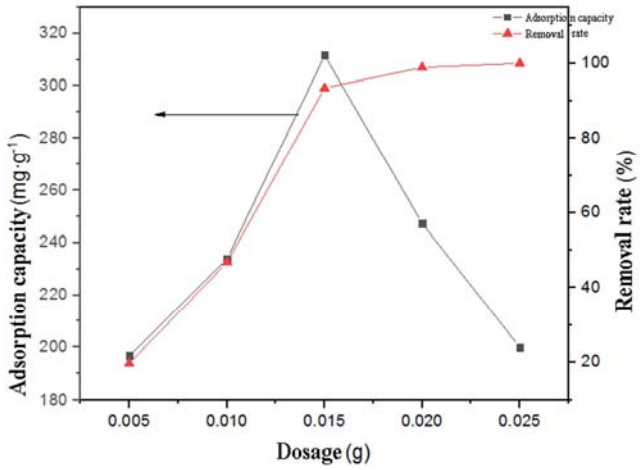

Figure 14. *The effect of MBC dosage on the removal of P4R.*

3.4.2. Influence of pH Values

It can be seen from the figures 15 and 16 that the adsorption capacity and removal rate of MB by the adsorption material increase with the increase of pH, and the adsorption capacity and removal rate increase from 449.8 $mg \cdot g^{-1}$ and 89.96% at pH 4 to 499.95 $mg \cdot g^{-1}$ and 99.99% at pH 12. Among them, the adsorption capacity and removal rate were greatly improved from pH 8 to 11, and reached the maximum at pH 12, with the adsorption capacity and removal rate reaching 499.95 $mg \cdot g^{-1}$ and 99.99% respectively.

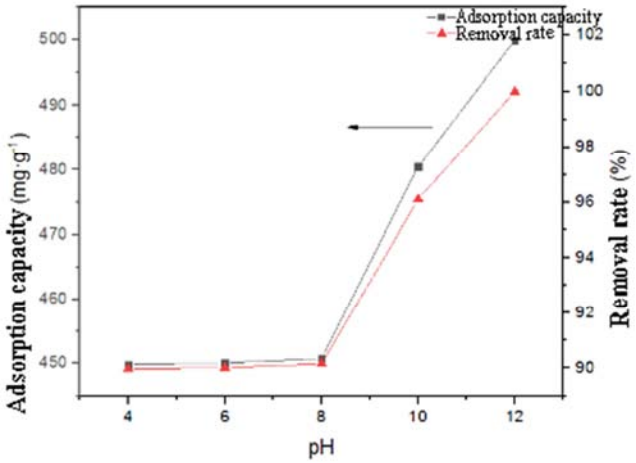

Figure 15. *The effect of pH on the removal of MB.*

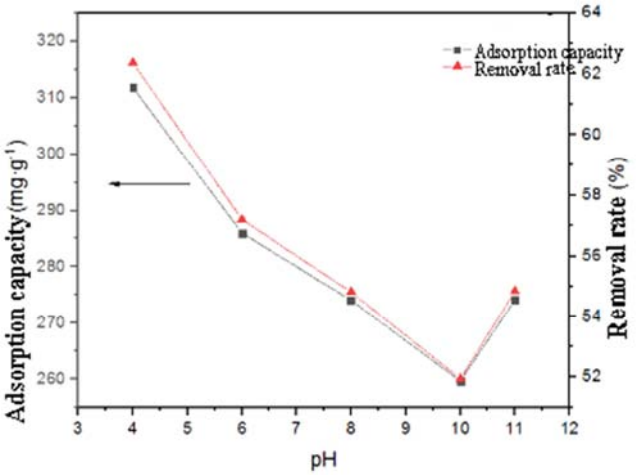

Figure 16. *The effect of pH on the removal of P4R.*

PH will affect the surface charge of biochar, occupy adsorption sites, and then affect the electrostatic adsorption effect between adsorption materials and dye molecules. When the pH value is low, there is more H^+ in the solution, and functional groups on the surface of biochar, such as hydroxyl and amine groups, are protonated with a large number of positive charges, which will repel MB molecules with positive charges, resulting in their inability to effectively adsorb on biochar. At the same time, If the pH is too low, Fe_3O_4 will decompose and release cationic iron, which will compete with MB for adsorption together with excess H^+, occupying limited adsorption sites, and will also reduce its adsorption capacity. With the increase of pH, the surface protonation degree of biochar decreases, and the competition of adsorption sites decreases, which is beneficial to the adsorption of MB, and the adsorption capacity and removal rate also increase.

As for P4R, with the increase of pH, the adsorption capacity and removal rate showed a downward trend in general, from 311.8 $mg \cdot g^{-1}$ and 62.36% at pH 4 to 259.65 $mg \cdot g^{-1}$ and 51.93% at pH 10, and the removal rate and adsorption rate were 274.15 mg at pH 11.

P4R dye molecules are negatively charged in water. Under

the condition of low pH, $-NH_2$ on the material surface is protonated to form $-NH^{3+}$, which is beneficial to the adsorption of anionic dyes. At the same time, the combination of $-SO^{3-}$ and H^+ on the dye molecule will hinder its combination with adsorption materials, and the two will form a competitive relationship. At lower pH, when the protonation of $-NH_2$ is dominant, the adsorption amount and removal rate of the dye by the adsorption material will be increased. With the increase of pH, the degree of protonation decreases, and the negative charge on the surface of the material increases, forming repulsion force with dye molecules and competitive adsorption relationship with them, which is not conducive to adsorption. Therefore, for P4R, lower pH is more favorable for adsorption. At pH 11, the increase of adsorption capacity and removal rate is due to the change of molecular structure of P4R in the environment of higher pH, and the remaining adsorbed P4R in the solution cannot be detected, which leads to the low measurement concentration and the increase of adsorption capacity and removal rate.

3.4.3. Adsorption Isotherm

The fitting curves of Langmuir and Freundlich adsorption models of MB adsorbed by MBC are shown in Figures 17 and 18, and the relevant fitting data are shown in Table 2.

Table 2. *MBC adsorption isotherm parameters for MB.*

Temperature (°C)	Q_{me} (mg·g^{-1})	Langmuir			Freundlich		
		Q_{max} (mg·g^{-1})	K_l (L·mg^{-1})	R_{adj}^2	$\frac{1}{n}$	K_f (mg·g^{-1})	R_{adj}^2
15	416.95	417.46	0.995	0.9980	0.1026	259.20	0.8326
25	458.9	447.90	10.17	0.9717	0.0818	314.87	0.9324
35	465.6	456.08	44.83	0.9755	0.0702	339.02	0.9477

Note: "Q_{me}" is the experimental data, mg·g^{-1}.

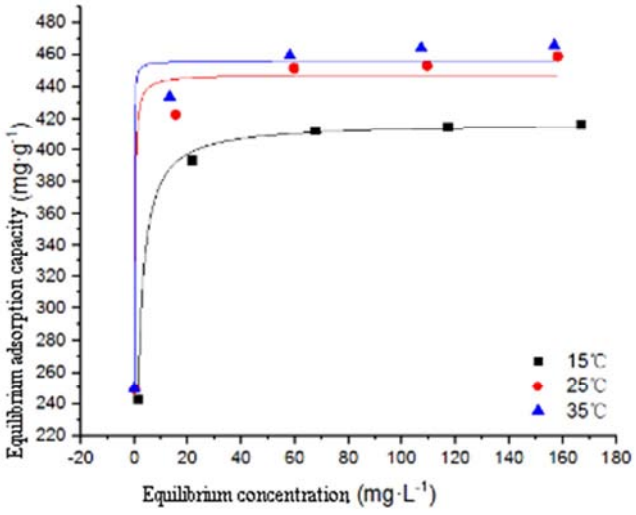

Figure 17. *Langmuir adsorption model.*

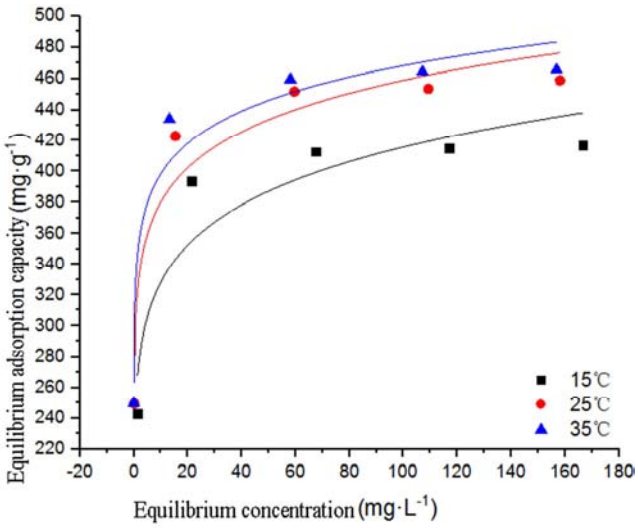

Figure 18. *Freundlich adsorption model.*

It can be seen from Table 2 that the correlation coefficients of Langmuir model are all greater than those of Freundlich model, all of which are above 0.97, which indicates that Langmuir model is more suitable for explaining the adsorption of MB by MBC. In addition, compared with the measured Q_{me}, the Q_{max} fitted by the fitting curve is close, with a difference of 0.12%-2.39%, with little difference. Therefore, the adsorption of MB on MBC is more in line with the assumption of Langmuir model and belongs to monolayer adsorption. The dye molecules are evenly distributed on MBC surface. With the increase of temperature, K_l increases, which is favorable for adsorption, which is an endothermic process. The values of 1/n calculated by Freundlich model are all around 0.1, indicating that adsorption is easy.

The fitting curves of Langmuir and Freundlich adsorption models of MBC adsorption P4R are shown in Figures 19 and 20, and the relevant fitting data are shown in Table 3.

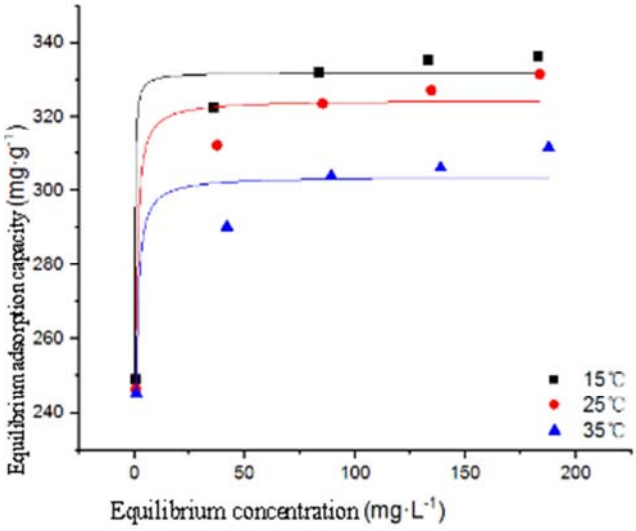

Figure 19. *Langmuir adsorption model.*

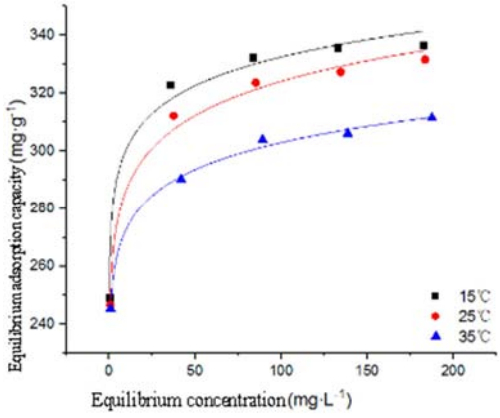

Figure 20. *Freundlich adsorption model.*

From Table 3, the correlation coefficients of Freundlich model are all above 0.98, which is larger than that of Langmuir model, indicating that Freundlich model is more suitable for explaining the adsorption of P4R by MBC. In addition, compared with the experimental measured value Q_{me}, the Q_{max} fitted by the fitting curve still has a certain gap, which is smaller than the measured value, but it is also very close. The adsorption of P4R on MBC is more in line with the hypothesis of Freundlich model, It belongs to multilayer adsorption. With the increase of temperature, K_f decreases, and adsorption is an exothermic process. The values of 1/n are all less than 0.1, indicating that adsorption is easy.

Table 3. *MBC adsorption isotherm parameters for P4R.*

Temperature (°C)	Q_{me} (mg·g^{-1})	Langmuir			Freundlich		
		Q_{max} (mg·g^{-1})	K_l (L·mg^{-1})	R_{adj}^2	$\frac{1}{n}$	K_f (mg·g^{-1})	R_{adj}^2
15	336.6	332.04	18.78	0.9732	0.044	271.81	0.9862
25	331.55	324.62	4.56	0.9531	0.053	253.43	0.9880
35	311.55	303.85	4.43	0.9011	0.045	245.99	0.9958

Note: "Q_{me}" is the experimental data, mg·g^{-1}.

3.4.4. Adsorption Thermodynamics

The conversion data with K_l and K^0 are shown in Table 4, and the thermodynamic parameters of 4, MBC adsorbing MB and P4R are shown in Tables 4 and 5.

Table 4. *K_l and K^0 data conversion.*

MB		P4R	
K_l	K^0	K_l	K^0
0.995	372030.5	18.78	11351946.6
10.17	3802563	4.56	2756383.2
44.83	16761937	4.43	2677802.1

Note: The molecular weight of MB is 373.9 g·mol^{-1} and that of P4R is 604.47 g·mol^{-1}.

Table 5. *Adsorption thermodynamic parameters of MBC for MB.*

Temperature (K)	ΔG^0 (kJ·mol^{-1})	ΔS^0 (kJ·mol^{-1}·K^{-1})	ΔH^0 (kJ·mol^{-1})
288	-30.7127		
298	-37.5382	0.5942	140.12
308	-42.5965		

From Table 5, it can be seen that the adsorption ΔG^0 of MBC to MB is less than zero, and ΔS^0 and ΔH^0 are greater than zero, which indicates that the adsorption reaction proceeds spontaneously at high temperature. ΔG^0 is less than zero, and the adsorption reaction is spontaneous, and with the increase of temperature, ΔG^0 becomes smaller and smaller, which is beneficial to adsorption.

ΔH^0=140.12 kJ·mol^{-1} is greater than 25 kJ·mol^{-1}, which belongs to chemical adsorption, and ΔG^0 gradually approaches and exceeds the vicinity of -40 kJ·mol^{-1} with the increase of temperature, which comprehensively shows that physical adsorption and chemical adsorption may exist at the same time, and the adsorption process is more inclined to chemical adsorption with the increase of temperature.

ΔS^0 is a positive value, which is a process of increasing entropy, and the degree of chaos increases. Molecules promote adsorption by replacing water molecules from MBC surface, that is, water molecules desorb from the surface of adsorption material, resulting in the increase of entropy.

ΔH^0 is greater than zero, which indicates that the adsorption process is an endothermic process, and the temperature rise is beneficial to adsorption, which is consistent with the previous research on temperature influence and adsorption isotherm.

Table 6. *Adsorption thermodynamic parameters of MBC for P4R.*

Temperature (K)	ΔG^0 (kJ·mol^{-1})	ΔS^0 (kJ·mol^{-1}·K^{-1})	ΔH^0 (kJ·mol^{-1})
288	-38.8973		
298	-36.741	-0.0599	-52.708
308	-37.8998		

As for the adsorption of P4R by MBC, as shown in Table 6, ΔG^0 is less than zero, ΔS^0 and ΔH^0 are less than zero, which indicates that the adsorption reaction proceeds spontaneously at low temperature. ΔG^0 is less than zero. With the increase of temperature, ΔG^0 tends to increase, which is not conducive to adsorption.

ΔG^0 is close to -40 kJ·mol^{-1}, and ΔH^0 is less than 25 kJ·mol^{-1}, which indicates that chemical adsorption and physical adsorption may exist at the same time.

ΔS^0 is negative, which indicates that it is a process of decreasing entropy and disorder. Dye molecules are

constantly adsorbed, and move from three-dimensional motion to two-dimensional motion, with the degree of order increasing and entropy decreasing.

The negative value of ΔS^0 indicates that the adsorption process is exothermic, and the temperature rise is not conducive to adsorption, which is consistent with the previous study of temperature influence and adsorption isotherm.

3.4.5. Adsorption Features

(i). The Adsorption Saturated Time

Figure 21 and Figure 22 show the adsorption saturated curves of the MBC for MB and P4R at three concentrations of 50 $mg \cdot L^{-1}$, 100 $mg \cdot L^{-1}$ and 150 $mg \cdot L^{-1}$ with T as abscissa and the adsorption amount at time T as ordinate.

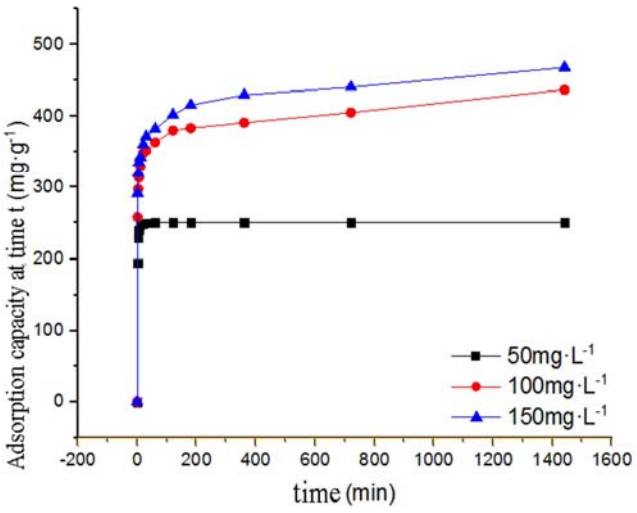

Figure 21. *The effect of contact time on the removal of MB.*

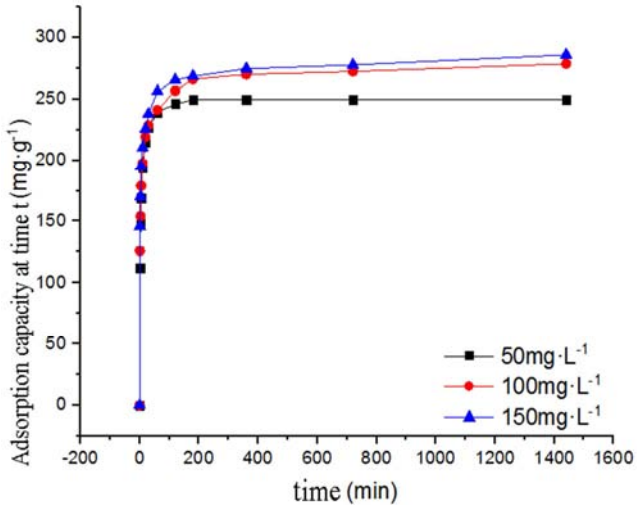

Figure 22. *The effect of contact time on the removal of P4R.*

As can be seen from Figure 21 and Figure 22, the adsorption capacity of the two dyes increases with time, and the adsorption is faster in the early stage, then slows down and gradually reaches the adsorption equilibrium. For MB, 30min at lower concentration is close to adsorption equilibrium, and 180min at higher concentration. For P4R, the three concentrations are 120min. At the initial stage of adsorption, MBC has sufficient adsorption sites on the surface, and the dye concentration is higher and the mass transfer rate is higher, so the adsorption rate in the early stage is faster. With the extension of time, the adsorption sites on the surface layer are gradually occupied, the concentration decreases, the driving force decreases, and the dye molecules are repelled by the adsorbed dye molecules when they diffuse into MBC, which makes the adsorption process slow.

(ii). Adsorption Kinetics

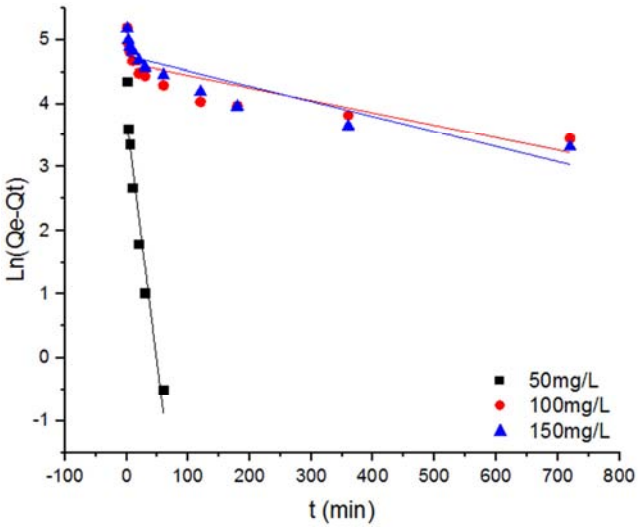

Figure 23. *The pseudo-first-order adsorption kinetic model for the adsorption of MB onto MBC.*

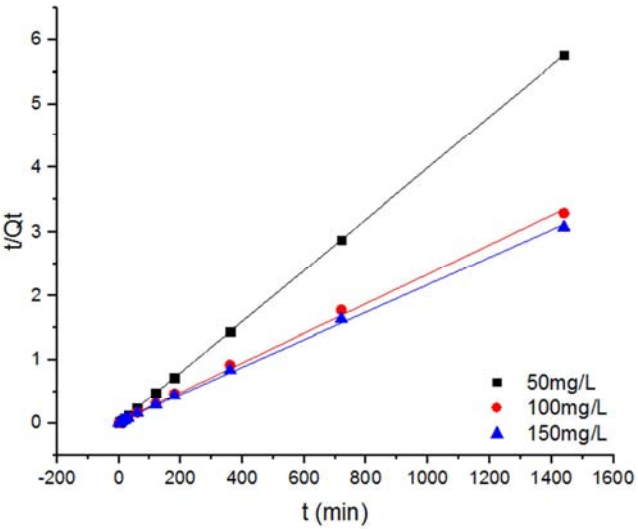

Figure 24. *The pseudo-first-order adsorption kinetic model for the adsorption of MB onto MBC.*

The fitting curves of quasi-first-order equation and quasi-second-order equation of MB adsorption by MBC are shown in Figures 23 and 24, and the fitting related data are shown in Table 7.

Table 7. *Adsorption kinetic parameters of MBC for MB.*

Concentration ($mg·L^{-1}$)	q_{exp} ($mg·g^{-1}$)	Quasi-first-order equation			Quasi-secondary equation		
		q_e ($mg·g^{-1}$)	k_f (min^{-1})	R_{adj}^2	q_e ($mg·g^{-1}$)	k_s (g·(mg·min)-1)	R_{adj}^2
50	249.95	42.72	7.75×10-2	0.92613	250.00	1.11×10-2	0.99999
100	436.75	103.75	1.96×10-3	0.66646	432.90	1.86×10-4	0.99838
150	467.85	115.90	2.38×10-3	0.78774	465.12	1.95×10-4	0.99885

Table 8. *Adsorption kinetic parameters of MBC for P4R.*

Concentration ($mg·L^{-1}$)	q_{exp} ($mg·g^{-1}$)	Quasi-first-order equation			Quasi-secondary equation		
		q_e ($mg·g^{-1}$)	k_f (min^{-1})	R_{adj}^2	q_e ($mg·g^{-1}$)	k_s ($g·(mg·min)^{-1}$)	R_{adj}^2
50	249.95	76.72	2.85×10-2	0.96248	250.63	1.85×10-3	0.99999
100	278.55	67.88	4.21×10-3	0.68742	278.55	5.54×10-4	0.99986
150	285.75	63.75	3.63×10-3	0.65411	284.90	5.40×10-4	0.99978

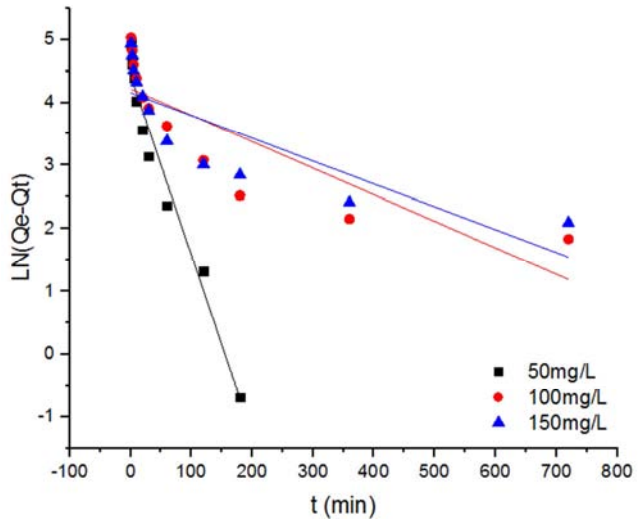

Figure 25. *The pseudo-second-order adsorption kinetic model for the adsorption of P4R onto MBC.*

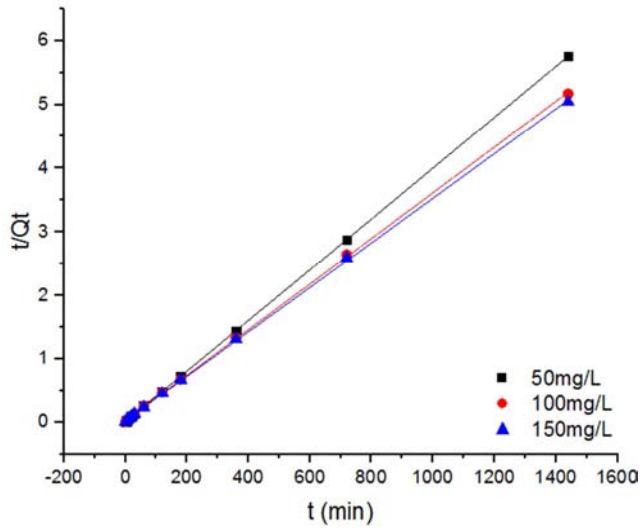

Figure 26. *The pseudo-second-order adsorption kinetic model for the adsorption of P4R onto MBC.*

The fitting curves of quasi-first-order equation and quasi-second-order equation of MBC adsorption P4R are shown in Figures 25 and 26, and the fitting data are shown in Table 8.

According to the data in Table 7, the adsorption of MB by MBC is more in line with the quasi-second-order adsorption kinetic model. R_{adj}^2 of the three quasi-second-order equations of concentration fitting are all above 0.99, and the fitting degree is higher than that of quasi-first-order equations. In addition, the theoretical adsorption capacity calculated by fitting the quasi-second-order adsorption kinetic equation is very close to the measured value. The quasi-second-order adsorption kinetic model can better explain the whole adsorption process.

According to the data in Table 8, the adsorption of P4R by MBC is more in line with the quasi-second-order adsorption kinetic model. R_{adj}^2 of the three-concentration fitting quasi-second-order equations are all above 0.999. Compared with the quasi-first order equation, the fitting degree is higher. In addition, the theoretical adsorption capacity calculated by fitting the quasi-second-order adsorption kinetic equation is very close to the measured value. The quasi-second-order adsorption kinetic model can better explain the whole adsorption process.

4. Conclusions

Pine needles were impregnated with KOH and carbonized to prepare pine needle biochar SBC. The preparation conditions were explored, and the best materials were screened out by comparison of adsorption effects to prepare magnetic biochar, which was further characterized and studied on adsorption performance. The conclusions are as follows:

(1) 8SBC impregnated with 8 $mol·L^{-1}$ KOH solution at 800°C has the best adsorption effect and larger specific surface area. The surface of magnetic biochar MBC prepared on the basis of 8SBC contains functional groups such as -OH, -C-H, -N-H, C-O etc. And has rich pore structure, with a specific surface area of 785.7522 $m^2·\ g^{-1}$, and the crystal structure is more orderly after negative magnetism. SEM, XRD and EDS show that Fe_3O_4 particles are successfully loaded, and the specific saturation magnetization is 15.9 $ome·g^{-1}$, which can be effectively separated.

(2) In the experimental range, the adsorption capacity of MBC for MB increased with the increase of

concentration, and the removal rate showed a downward trend, while the adsorption capacity and removal rate increased with the increase of time. Adsorption equilibrium can be reached in 30min at lower concentration, and it is close to adsorption equilibrium in 180min at higher concentration. High temperature and high pH are beneficial to MBC adsorption of MB, and the removal rate and adsorption capacity can be kept at a high level when the dosage is 0.01g/L.

(3) Within the experimental range, the adsorption capacity of MBC for P4R increased with the increase of concentration, and the removal rate showed a downward trend, while the adsorption capacity and removal rate increased with the increase of time. All three concentrations were close to adsorption equilibrium in 120min. Low temperature and low pH are favorable for MBC to adsorb P4R, and the removal rate and adsorption capacity can be kept at a high level when the dosage is 0.015g.

(4) The results of adsorption isotherm, thermodynamics and kinetics show that Langmuir model can better describe the adsorption process of MBC to MB, which belongs to single-layer adsorption, while the Freundlich model can better describe the adsorption process of MBC to P4R, which belongs to multi-layer adsorption. The experimental values of the maximum equilibrium adsorption capacity of MBC and P4R are 465.6 $mg \cdot g^{-1}$ and 336.6 $mg \cdot g^{-1}$ respectively. The adsorption process of MB is spontaneous adsorption at high temperature, which is a process of endothermic and entropy increasing. P4R is spontaneous adsorption at low temperature, which is a process of exothermic and entropy reduction. All of them conform to the quasi-second-order adsorption kinetic model, and there is an intra-particle diffusion process, which is influenced by various adsorption mechanisms.

(5) It has good adsorption effect on various dyes, and the adsorption of cationic dyes is slightly better than that of anionic dyes. Without activation, regeneration and recycling, the adsorption effect of MB decreased obviously, and the adsorption capacity of P4R increased.

References

[1] Grégorio, Crini. Non-conventional. low-cost adsorbents for dye removal: a review. [J]. Bioresource technology, 2006, 97 (9): 1061-85.

[2] Hui, Ma, Pu. A highly efficient magnetic chitosan “fluid” adsorbent with a high capacity and fast adsorption kinetics for dyeing wastewater purification [J]. Chemical engineering journal, 2018, 345: 556-565.

[3] Sen, S. K., Raut. Fungal decolouration and degradation of azo dyes: A review [J]. Fungal biology reviews, 2016, 30 (3): 112-133.

[4] Zhang, O’Connor, Wang, et al. A green biochar/iron oxide composite for methylene blue removal [J]. Journal of Hazardous Materials, 2020, 384.

[5] An, Qiang, Zhao, et al. An alkali modified biochar for enhancing Mn^{2+} adsorption: Performance and chemical mechanism [J]. Materials Chemistry and Physics, 2020, 248.

[6] Umran, Tezcan, Un, Oduncu, et al. Adsorption of Disperse Orange 30 dye onto activated carbon derived from Holm Oak (Quercus Ilex) acorns: A 3 (k) factorial design and analysis. [J]. Journal of Environmental Management, 2015, 155: 89-96.

[7] Azargohar R, Dalai A K. Steam and KOH activation of biochar: Experimental and modeling studies [J]. Microporous & Mesoporous Materials, 2008, 110 (2-3): 413-421.

[8] Mohammed J, Nasri N S, Zaini M, et al. Comparison on the Characteristics of Bio-Based Porous Carbons by Physical and Novel Chemical Activation [J]. Applied Mechanics and Materials, 2014, 554.

[9] Tezcan, Un, U, Erginel N, et al. Adsorption of Disperse Orange 30 dye onto activated carbon derived from Holm Oak (Quercus Ilex) acorns: A 3k factorial design and analysis [J]. Journal of Environmental Management, 2015, 155: 89-96.

[10] Trakal, Veselská, Šafařík. Lead and cadmium sorption mechanisms on magnetically modified biochars [J]. Bioresource technology, 2016, 203: 318-2.

[11] Mohammad Ameera F., Mourad Aya A-H. I., Galiwango Emmanuel et al. Effective and sustainable adsorbent materials for oil spill cleanup based on a multistage desalination process [J] Journal of Environmental Management, 2021, 299.

[12] Xiuyu He, Zhijia Zhao, Yuhua Song Active control for flexible mechanical systems with mixed deadzone-saturation input nonlinearities and output constraint [J] Journal of the Franklin Institute, 2019, 356 (9).

[13] Lee Jae-In, Kim Jeong-Man, Yoo Soo-Cheul et al. Restoring phosphorus from water to soil: Using calcined eggshells for P adsorption and subsequent application of the adsorbent as a P fertilizer [J] Chemosphere, 2022, 287 (P3).

[14] Kayranli Birol Mechanism of interaction and removal of zinc with lignocellulosic adsorbents, closing the cycle with a soil conditioner [J] Journal of King Saud University - Science, 2021, 33 (8).

[15] Mei Yanglu, Xu Jin, Zhang Yin et al. Effect of Fe–N modification on the properties of biochars and their adsorption behavior on tetracycline removal from aqueous solution [J] Bioresource Technology, 2021, 325.

[16] Chen Juan, Liu Shanshan, Ge Heyi et al. A hydrophobic bio-adsorbent synthesized by nanoparticle-modified graphene oxide coated corn straw pith for dye adsorption and photocatalytic degradation [J] Environmental Technology, 2020, 41 (27).